Iran J Sci Technol Trans Sci
https://doi.org/10.1007/s40995-021-01183-4

RESEARCH PAPER

Role of TiO_2/ZnO Nanofillers in Modifying the Properties PMMA Nanocomposites for Optical Device Applications

N. B. Rithin Kumar[1] · Santhosha Acharya[2] · A. Alhadhrami[3] · B. M. Prasanna[4] · S. C. Gurumurthy[5] · Sangeetha Bhat[2]

Received: 5 May 2021 / Accepted: 15 July 2021

Abstract
In the present study, ZnO and TiO_2 nanofillers with different concentrations are integrated into the PMMA matrix on the glass substrate using a cost-effective spin coating technique. XRD investigations show the maximum crystalline complexity of 24.56% crystallinity with a rise in filler concentration up to x = 10 wt%. SEM and EDS studies signify the homogenous distribution and compatibility of nanofillers in the host PMMA matrix. Raman spectroscopy demonstrates the influential transition peak identified at 840 cm^{-1} for an optimized filler concentration of x = 10wt%. The C=O and C–O of host PMMA are out of plane bending with an estimated PED of $64\eta_{C=O} + 16\eta_{C-O}$, indicating a pivotal role in filler and matrix complex formulation. Optical studies show enhancement in transmittance with a rise in filler concentration up to 10 wt%, offering a maximum value of nearly 85%. The course also emphasizes the solid antireflection nature with a decreased bandgap value to 1.94 eV. The observed upsurge in optical conductivity suggests the number of free charges present in the nanocomposite films. The increase in optical conductivity with a reduced energy bandgap of these PMMA/$(15 - x)$ ZnO $(x)TiO_2$ shows a promising contender for optical device applications.

Keywords PMMA · Nanofillers · Raman spectroscopy · Optical studies · TiO_2 · ZnO

1 Introduction

In recent years, integrating one dimension, two dimensions, three-dimensional, and their combination as nanofillers into the polymer matrix has become a sustainable route to enhancing the host polymer's physical and chemical properties. The main reasons for using nanofillers have a large surface to volume ratio, which increases the number of fillers–matrix interactions, thus increasing the overall material properties effects. However, specific challenges such as interface and compatibility between the nanofiller and matrix need to be addressed to obtain the desired properties. Further, optimized integration would enhance the optical, electrical, and mechanical properties of the nanocomposites. Thus, this optimized integration would open up new avenues for applications in electronics, optical, medical devices, etc. (Hong et al. 2009; Agarwal et al. 2014; Aboulouard et al. 2020; Bai et al. 2014).

In recent years, PMMA is the most favorable matrix material out of many synthetic and natural polymers due to its versatile physio-chemical properties such as light-weight, higher softening point, shatter-resistant, high impact strength, dimension stability, wear as well as scratch resistance (Huda et al. 2019; Mauro et al. 2017). Further, PMMA is compatible with nanosize materials and is relatively easy to achieve uniform nanofiller dispersion

✉ N. B. Rithin Kumar
rithinkumar@ajiet.edu.in

1 Department of Physics, A J Institute of Engineering and Technology, (Affiliated to Visvesvaraya Technological University, Belagavi), Mangaluru, Karnataka, India

2 Department of Physics, Yenepoya Institute of Technology, (Affiliated to Visvesvaraya Technological University, Belagavi), Moodabidri, Mangaluru, Karnataka, India

3 Department of Chemistry, College of Science, Taif University, P. O. Box 11099, Taif 21944, Saudi Arabia

4 Department of Chemistry, Jain Institute of Technology, (Affiliated to Visvesvaraya Technological University, Belagavi), Davanagere, Karnataka, India

5 Department of Physics, Nanomaterials and Polymer Physics Lab, Manipal Institute of Technology, Manipal, Karnataka, India

Published online: 31 July 2021

in the matrix. Apart from these, PMMA has extraordinary resistance to hot sunshine exposure, and its properties will not change with time. Hence, PMMA is an appropriate host material in the antireflection coating (ARC) owing to its overall thermal stability (− 70 °C to 100 °C), a refractive index of 1.49 with a reasonable degree of compatibility, and highly effective reflectance generating demands in the field of solar photovoltaic devices. Apart from these, PMMA films are utilized for constructing Light bulbs, car window panels, and mobile phones in which aids enhance light-producing capacity.

Furthermore, it is often utilized to fabricate lights due to its transparency and optical characteristics (Alsaad et al. 2019). Therefore, it is anticipated that the synthesis of distinctive characteristics of PMMA with nanofillers in specific well-designed composites would lead to materials of keen interest from conceptual as well as technical standpoints. The transparent thermoplastic polymers Poly (methyl methacrylate) (PMMA) have valuable features, cheap costs, and investigation of PMMA filled with metal oxide nanocomposites have become continuous research (Kobayashi et al. 2009; Lim et al. 2005; Kumar et al. Aug 2009). Although the dielectric stability for PMMA-ceramic composites (Purova et al. 2015; Su et al. 2014; Basahel et al. 2012) is modest, it substantially has a lower dielectric loss. Therefore, PMMA, when filled with nanofillers such as TiO_2 (Titanium oxide), ZnO (Zinc Oxide), nurture the hybrid nanocomposites finding numerous applications in the field of biomedical, solar, optoelectronic devices, and many more.

There are multiple reports on the preparation of PMMA-ZnO and PMMA TiO_2 nanocomposite thin films by different coating techniques (Stefanescu et al. 2010; Mauro et al. 2016; Khan 2015). Hence, PMMA filled with these two unique nanoparticles has distinct and exciting features that drive us to examine and comprehend their creation and development mechanisms and track the crucial loading quantity. The spin coating technique is employed in many preparation methods due to its simple process and cost-effective approach to obtain uniform coating on the substrate. Filling of host PMMA matrix with TiO_2 (Titanium oxide) and ZnO (Zinc Oxide) nanofillers using spin coating method is unique and proliferates the enactment of both physical and chemical properties of PMMA nanocomposites.

The present work emphasizes the preparation of PMMA-ZnO: TiO_2 hybrid nanocomposites using a spin coating method with varied concentrations of ZnO and TiO_2 nanofillers. We have attempted in many experiments to identify the appropriate proportion of ZnO and TiO_2 nanofillers in a PMMA matrix to improve the characteristics compared to host PMMA polymers. Furthermore, the systematic investigation of the structural and optical properties has explored the possibility of nanocomposites for optical device applications.

2 Materials and Methods

2.1 Synthesis of ZnO Nanoparticles

Zinc nitrate hexahydrate (Zn(NO3)26H2O), Titanium tetra isopropoxide (TTIP), Poly (methyl methacrylate) (PMMA) having a molecular weight of 3,50,000 g/mol are procured from Sigma Aldrich, Germany, 1,2-Dicholoroethane procured from Merck, India. The zinc nitrate hexahydrate is mixed with 350 mL deionized water stirred continuously using a magnetic stirrer at 300 rpm for 1 h. The mixture is treated with ammonia (25%) until the solution evolved from turbid to clear. The resultant concentrate was refluxed for 4 h under vigorous stirring for the formation of ZnO nanoparticles. The settled product is centrifuged and washed repeatedly until the pH value of the filtrate is 7. The obtained product is dried in air at 400 °C for 4 h, yields ZnO nanopowder (Mauro et al. 2017).

2.2 Synthesis of TiO_2 Nanoparticles

The synthesis of anatase TiO_2 nanoparticles is done using TTIP hydrolysis in 2-propanol with myristic acid as a capping agent employing an adjusted sol–gel process (Mardare and Rusu 2004). A 5 ml of TTIP is mixed with a 30 ml solution of 2-propanol for a molar ratio of 1:6 concerning myristic acid. The stirring rate of 500 rpm is carried out for 4 h until a white milky sol is obtained. The obtained sol solution is kept in the air for one day to undergo the gelation process. The white gel was filtered using Watmann Nylon filter paper, and the residue is washed until the pH of the filtrate reduces to a neutral value. The obtained white moisture substance is dried at 200 °C for 10 h, yield TiO_2 nanoparticles.

2.3 Substrate Cleaning

Out of many substrates cleaning methods, we have adopted the organic solvent process. Initially, a glass substrate of length 2.9 cm, width 1.2 cm, and thickness 1.2 mm was taken and washed with soap water. Further, the substrate is degreased using 1-propanol and kept for sonication in probe ultrasonicator for 20 s over 20 times with the interval of 20 s having the power of each pulse 35%. Further, it is sonicated using methanol and followed by acetone for 10 min, respectively. The substrate is then washed with deionized water and then again placed in a beaker filled with deionized water and sonicated again, as mentioned

above. Finally, the substrate is dried overnight in a dust-free oven maintained at 50 °C.

2.4 Film Coating

1.6 g of PMMA is dissolved in 80 ml of 1,2-Dicholoroethane solution. Later, remnant viscous PMMA is filled with $(15 - x)$ZnO and (x) TiO_2 nanoparticles for x = 0, 1, 5, 7.5, 10, 14, and 15 wt%. The filled nanoparticle PMMA solvent is sonicated for 10 s over ten times with an interval of 90 s at a temperature of 40 °C with 35% sonication power using probe ultrasonicator (PKS500FM, PCI analytics, India) for getting uniform dispersion. The solvent is coated onto a clean glass substrate using a spin coating unit (Model: HO-TH-05, HOLMARC Opto-Mechatronics Pvt Ltd, India). Further, 130 µL final solution is drop coated onto the glass substrate. The spin rate was kept at 2000 rpm with the acceleration of 2000 rpm, and time adjusted for 60 s. The coated samples are then heat-treated overnight, keeping in an oven at 50 °C. PMMA is a hydrophilic polymer that might absorb water from the atmosphere, affecting its physical properties. Thus, the prepared PMMA nanocomposite wrapped in a silver foil and are stored in a vacuum desiccator and used for further characterization.

2.5 Material Characterization

The film thickness was estimated using the DektaK stylus profilometer (Bruker). The average thickness of the deposited nanocomposites on the glass substrate is ~ 235 nm. The crystal structural analyses are done using 3rd generation Empyrean, Malvern Panalytical Multipurpose X-ray Diffractometer. Raman spectroscopy analysis is done by using WiTec alpha 300, Germany. Optical properties are carried out using Shimadzu UV visible Spectrometer. The structural images are obtained by Scanning electron microscopy (SEM) EVO 18 model and ALTO 1000 cryo attachment.

3 Result and Discussion

3.1 XRD Studies

Figure 1 represents the X-ray diffraction pattern of PMMA/$(15 - x)$ ZnO (x) TiO_2 for x = 0, 1, 5, 7.5, 10, 14, and 15 filler weight percentage concentration. The prominent broad peaks observed at 2θ = 20°–30° (crystalline peak) refer to the host PMMA matrix, and a broad peak indicates the formation of low dimension crystallites size. The addition of nanofillers into the PMMA matrix shifts the PMMA peaks toward the lower angle up to x = 10 wt%, indicating the enhancement in crystalline properties. The presence of less intense peaks indicates the amorphous predominant nature of nanocomposites.

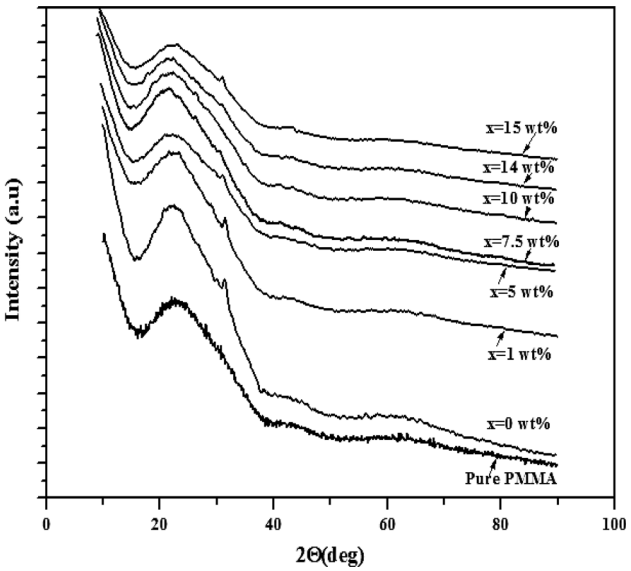

Fig. 1 X-ray diffraction pattern of PMMA: $(15 - x)$ ZnO (x) TiO2 for x = 0, 1, 5, 7.5, 10, 14, and 15 filler weight percentage concentration

Crystallite sizes of the embedded nanoparticles forming a complex conformation are estimated using the Debye–Scherrer formulation (Khanna et al. 2007),

$$D = \frac{k\lambda}{\beta \cos\theta} \tag{1}$$

where k is a constant having value equal to 0.9, which depends on the shape of the crystal and corresponding crystallographic planes, D is the average size or crystallite size of the particles, λ is the wavelength of x-rays, β is the full width at half maximum of X-ray profile, and θ is the Bragg angle. The percentage crystallinity of the PMMA nanocomposites is calculated using XRD patterns (Zidan 2003),

$$\%\ \text{Crystallinity} = \frac{(\text{total area of crystalline peaks})}{(\text{total area of all peaks})} \tag{2}$$

The micro strain produced in the PMMA entanglement on nanofiller producing a complex conformation is estimated using the relationship (Bhajantri et al. 2006),

$$\varepsilon = (\beta \cos\theta/4) \tag{3}$$

The dislocation density (δ) produced in the PMMA matrix filled with nanofillers are calculated using relation (Vos and Dhelsen 1979),

$$\delta = 1/D^2 \tag{4}$$

Table 1 represents the calculated crystalline parameters of PMMA: $(15 - x)$ZnO$(x)$$TiO_2$ for a different

Table 1 XRD parameters of PMMA/(15 − *x*) ZnO (*x*) TiO_2 for '*x*' nanofiller concentration

Filler concentration (*x*)	Crystallinity %	Crystallite size D (nm)	Microstrain ε (mm)	Dislocation density δ (10^{16} lines/m^2)	N(10^{17} m^{-2})
Pure PMMA	11.62	5.023	7.235	3.96	18.51
0 wt%	15.23	8.345	3.953	1.435	11.14
1 wt%	18.35	8.765	3.342	1.301	10.61
5 wt%	21.98	9.819	2.913	1.037	9.473
7.5 wt%	23.12	10.676	2.478	0.878	8.713
10 wt%	24.56	12.647	2.183	0.625	7.355
14 wt%	22.61	11.328	2.233	0.780	8.211
15 wt%	23.33	11.953	2.336	0.700	7.782

composition. Table 1 specifies the upsurge in the crystallite size up to *x* = 10 wt%; after that, it decreases. The rise in crystalline parameters is due to PMMA entanglement, with the added nanofillers forming a strong, complex configuration. Conversely, the dislocation density decreases with an increase in nanofiller percentage composition.

3.2 Raman Spectroscopy Studies

The Raman active vibrational modes of PMMA loaded with the desired loading nanofillers are analyzed in the range 300–800 cm^{-1} (Williamson and Smallman 1956). The band has demonstrated some significant improvement in loaded nanocomposites, indicating that the addition of '*x*' amount of ZnO and TiO_2 nanofillers modifies PMMA/(15 − *x*) crystalline structure ZnO (*x*) TiO_2 nanocomposites. The same is replicated in Fig. 2, signifying a broad range of peaks witnessed from 470 to 800 cm^{-1} refers to C–C as well as C–O is in-plane bending stretching vibrations of PMMA nanocomposites. The peak begins to appear from 482 cm^{-1} that indicates the nanofiller binds with host PMMA weak C–C and $C–CH_3$ are in-plane bending (β) with calculated potential energy distribution (PED) for each normal mode $70\beta_{C\text{-}C} + 12\beta_{C\text{-}CH3}$ (Giri et al. 2007). The slight increase in filler concentration for *x* = 1 wt%, the prominent vibrational peak observed at 395 cm^{-1}, refers to PMMA medium C–O, and C=O bonds are out of plane bending (η) PED associated with every normal mode is $62\eta_{C–O} + 14\eta_{C=O}$ (Khan 2015).

Further, enhancement in filler concentration up to *x* = 10 wt% the shifts the peaks heading toward the lower wavelength indicates the complex formation of nanofillers on PMMA's C–O and C=O bond, making it out of plane bending with PED of every normal mode $55\eta_{C–O-} + 11\eta_{C=O}$. The prominent transition peak witnessed at 840 cm^{-1} for optimized filler concentration x = 10 wt%

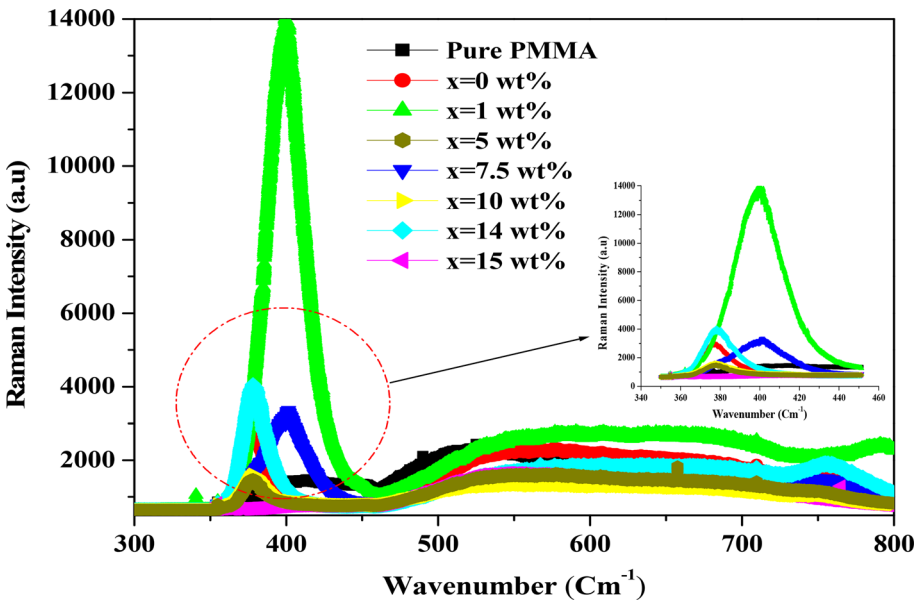

Fig. 2 Raman spectra of PMMA/(15 − *x*) ZnO (*x*) TiO_2 nanocomposites for different filler concentration

refers to C=O and C–O out of plane bending with an estimated PED of $64\eta_{C=O} + 16\eta_{C-O}$. The Raman shift observed in nanocomposites spectra may be a structural disorder, impurities, oxygen deficiency in addition to phonon confinement. The change in peaks toward lower-order indicates the growth in bond length transpired due to ZnO and TiO_2 nanofillers' expansion on the PMMA matrix, forming a complex conformation, thereby improving its crystalline parameters as quantified in XRD studies. Thus, changes observed in Raman spectra authorize the structural modification of PMMA after the incorporation of ZnO and TiO_2 nanoparticles.

3.3 Optical Studies

Figures 3 and 4 explore the optical absorption and transmittance spectra for specific TiO2 and ZnO composition in the PMMA matrix. Further, Fig. 5 shows the direct bandgap spectra of pure PMMA and PMMA/(15 − x) ZnO (x) TiO_2 nanocomposites filler proportion x = 0, 1, 5, 7.5, 10, 14, and 15 wt%. The absorption coefficient of PMMA nanocomposites was found to be negligible within the bandgap zone. However, its intensity increases with a decrease in wavelength. The negligible absorption co-efficiency of these hybrid nanocomposites demonstrates their appropriateness as the window layer of solar cells within the spectrum's visible portion. The transmittance spectra of filled PMMA/(15 − x) ZnO (x) TiO_2, compared with pure PMMA, shows an enhancement in transmittance with a rise in filler concentration up to 10 wt% delivering a maximum value of nearly 85%. This high transmittance may be due to nanofillers' percentage loading, size, and spatial distribution in the host PMMA matrix (Rosemal et al. 2010).

The study also shows that the filling of above 10 wt% nanofillers decreases the transparency substantially compared to the pure PMMA. It is evident from the graph that the clarity found its enhancement at higher wavelengths when compared to the lower wavelength region. The enhancement in the transmission is due to the increase in the complex configuration of the particle size of PMMA bonded by nanoparticles up to x = 10 wt%. The same is observed in XRD results, suggesting that transmission transpires when the particle size increases (Chang et al. 2011). This high transparency PMMA/(15 − x)ZnO (x) TiO_2 finds applicable in optical materials in optoelectronic devices.

Its optical absorption bandgaps are dictated from the UV–visible spectra by converting the spectra into Tauc's plots using frequency-dependent absorption coefficient provided by Mott and Devis (Mott and Devis 1979; Mott 1993). Therefore, plotting the absorption coefficient $(\alpha h\nu)^2$ with photon energy ($h\nu$) at ambient temperature has been seen as linear curve effectiveness. Such a direct action reflects the natural permissible transformations somewhere between the valence band and conduction band. The table compares the energy bandgap (E_g) for different filler concentrations of performance enhancers. The observed lower E_g of 1.91 eV for filler x = 10 wt% percent is

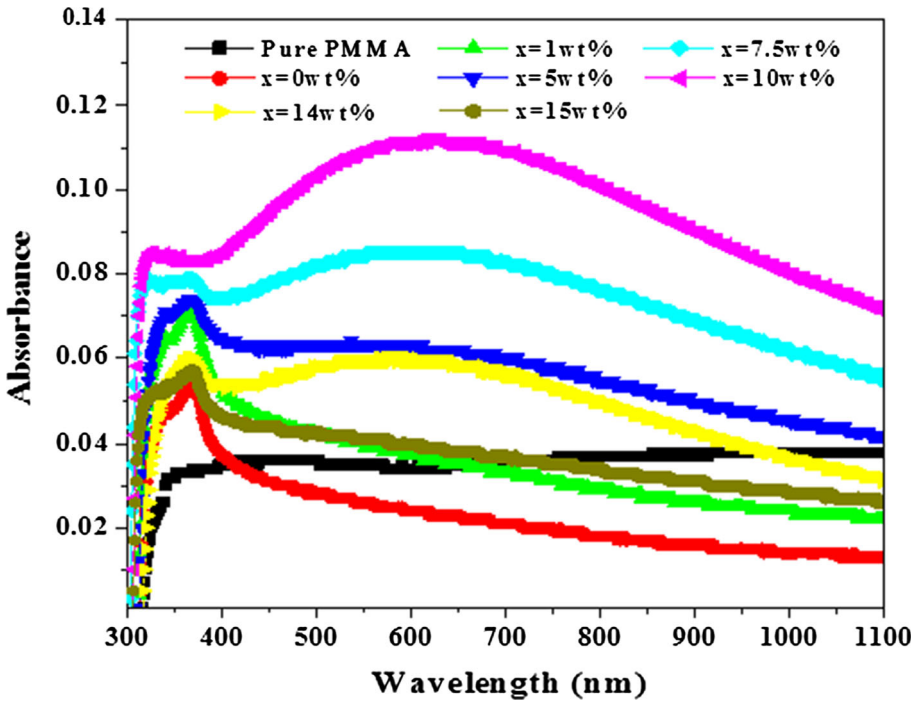

Fig. 3 Absorbance spectra of PMMA/(15 − x) ZnO (x) TiO_2 nanocomposites for different filler concentration

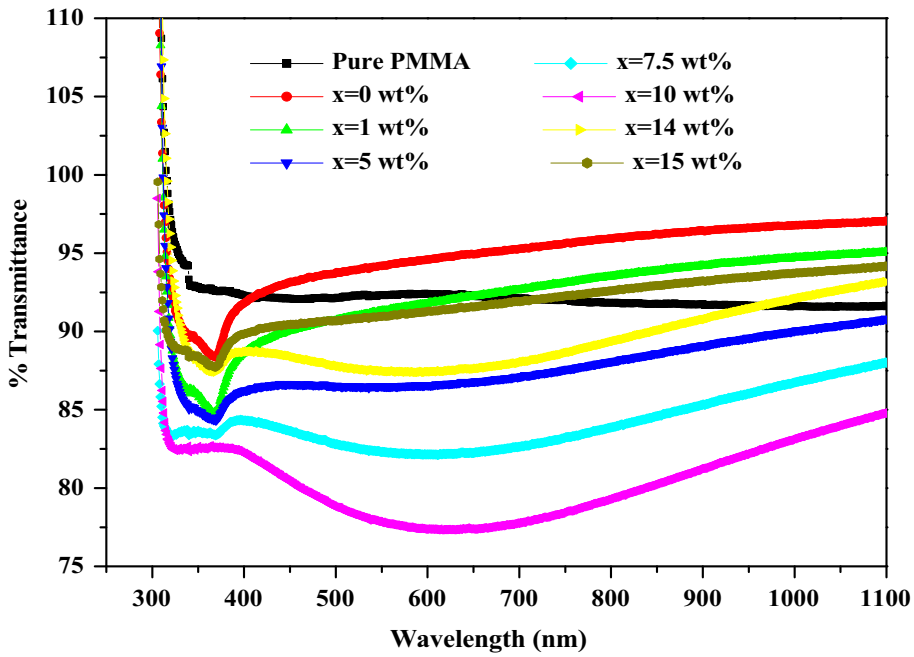

Fig. 4 Transmission spectra of PMMA/(15 − x) ZnO (x) TiO_2 nanocomposites for diverse filler concentration

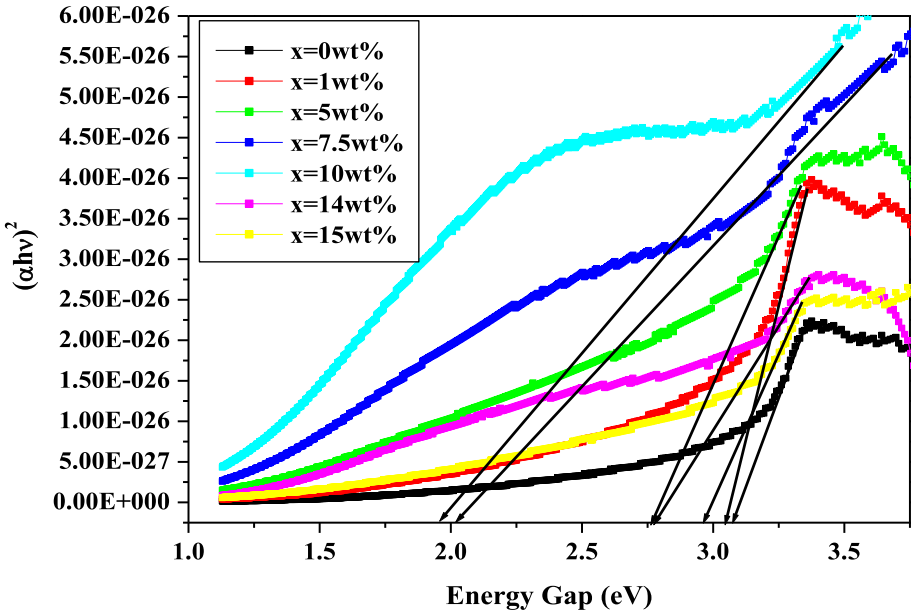

Fig. 5 Energy band gap of PMMA/(15 − x) ZnO (x) TiO_2 nanocomposites for different filler concentration

directly linked to the local complex formation between the interpenetrating PMMA chain and incorporated nanofillers. The ZnO/TiO_2 spin-coated thin membranes have a minimal optical 1.91 eV energy difference which is highly transparent and may be utilized for UV protection and solar panels. Nanofillers TiO_2 and ZnO introduced in the matrix form complexes with PMMA interpenetrating sporadic coils culminating in departed molecular mobility to create an interactive configuration. The nanofiller's critical volume generates a continuous network inside the hybrid polymer nanocomposite (Tauc 1972; Selim et al. 2005). This makes an isolated conduction transition in the percolation filler composition. Such influences improve the crystallinity of PMMA/(15 − x)ZnO (x) TiO_2 while significantly reducing the energy gap. The decline in E_g with the proliferation in Ti filler percentage (x = 10 wt% concentration) is due to Ti substitution in place of Zn in the lattice of ZnO in the PMMA matrix (Patil et al. 2009).

The presence of high reactive titanium-terminated anatase surface having declined energy bandgap less than 2 eV reduces the bandgap of PMMA nanocomposites up to the filler level x = 10 wt% (Dette et al. 2014). The Ti^{2+} ions incorporate into the PMMA matrix also substitute the Zn^{2+}, creating double ionized oxygen vacancies or

incorporation as interstitials, thereby decreasing the energy bandgap. The extinction coefficient is calculated using the relation (Rouaramadan and Hasan 2013),

$$k = \frac{\propto \lambda}{4\pi} \tag{5}$$

where α is the absorption coefficient of the PMMA nanocomposites. The coefficient of extinction in Fig. 6 shows a dispersion pattern reflecting the Sellmeier relation. The extinction coefficient originates from light absorption whenever the photon wavelength is more extensive or equivalent to the grain scale. The advantages of dispersing the grains improve with the rise in nanofillers concentration, often attributed to the increased grain size and added nanoparticle density.

The Skin depth shown in Fig. 7 represents the reduction in electromagnetic waves' intensity, subsequently itinerating a particular unit thickness (Al-Ammar et al. 2013).

$$\chi = \frac{\lambda}{2nk} \tag{6}$$

where λ refers to a wavelength of the photon, besides K is the extinction coefficient. The energy needed for the photon to infiltrate PMMA/$(15 - x)$ZnO (x) TiO_2 nanocomposite matrix evaluates optical conductivity, which can be measured using the relation,

$$\sigma = \frac{\alpha nc}{4\pi} \tag{7}$$

The number of free charges inside the PMMA filled nanocomposite matrix is evaluated from optical conductivity (Abdul-Gader 2013). Figure 8 indicates the enhancement in free charges up to optimum filler concentration x = 10 wt% and above the optical conductivity decreases.

Figure 8 also shows the optical conductivity of the synthesized PMMA nanocomposites improves in the higher energy zone and further heightens in the visible region due to free charges absorbing the photon energy (Choudhary and Nayak 2019). Further, toward the IR region, the optical conductivity decreases. This may be due to the trapping of photon energy in the free carries binds its motion inside the PMMA/$(15 - x)$ ZnO (x) TiO_2 hybrid nanocomposites. For optimum filler concentration of x = 10 wt%, the optical conductivity is maximum both in UV and the visible region, making the material for optical devices applications.

3.4 SEM and EDS Studies

Figure 9 extol the SEM image designating the surface characteristics of PMMA:$(15 - x)$ ZnO (x) TiO_2 polymeric films for efficient load composition at room temperature of x = 10 weight percentage. The SEM photograph is limited to 4000X magnification, which leads to the creation of the micro-crack in the images. Figure 9 gives the streamlined dispersion of TiO_2 and ZnO nanofillers in a typically designed PMMA monomer. The average dimension of ZnO nanofillers is 77 nm, and TiO_2 is 112 nm. The intercalation shows well, enacts the involvement of nanofillers in the composites materials. The formation of complex conformation between the PMMA host chain and ZnO/TiO_2 nanocomposites enhances the

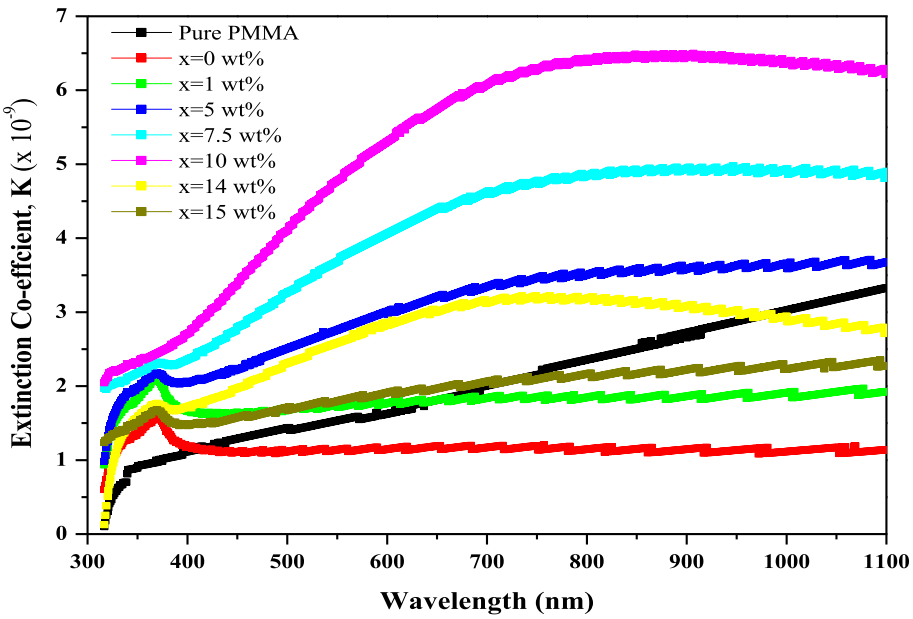

Fig. 6 Variation of extinction coefficient with the wavelength for PMMA/$(15 - x)$ ZnO (x) TiO_2 nanocomposites for different filler concentrations

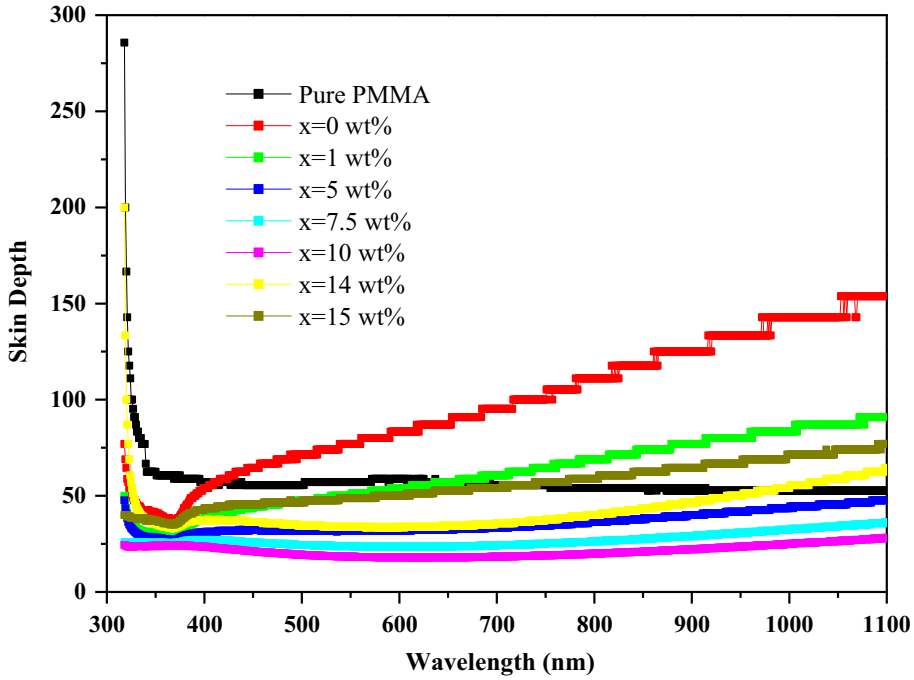

Fig. 7 Variation of skin depth with the wavelength for PMMA filled nanocomposites

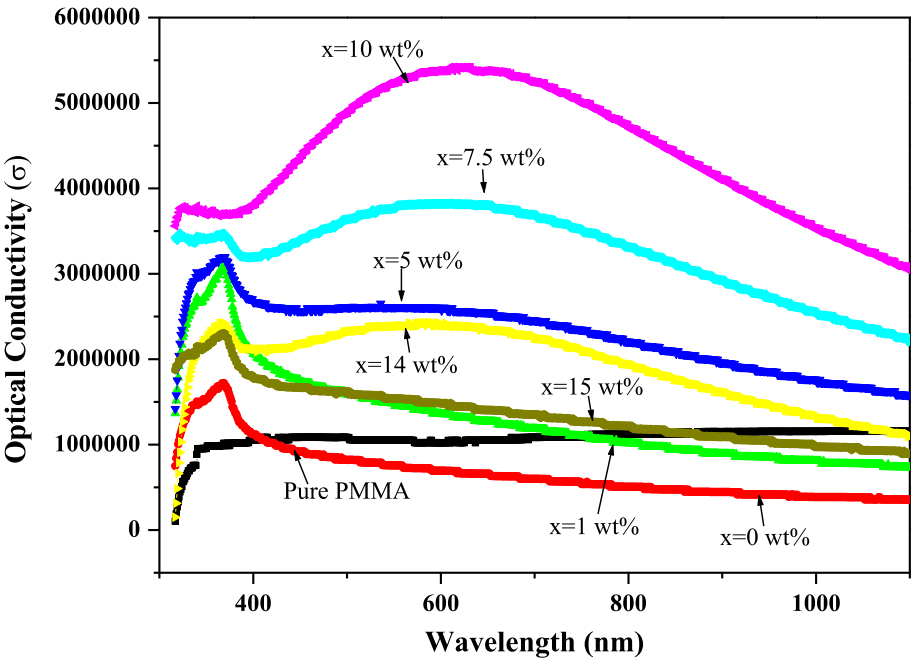

Fig. 8 Variation of optical conductivity with wavelength for PMMA/$(15 - x)$ ZnO (x) TiO_2 nanocomposites

microstructural variation observed in Fig. 9. A non-uniformity of the size arose in a few areas owing to conglomeration that significantly reduces higher surface energy enamored by isolated nano-sized fillers. Aside from these, the host PMMA matrix exhibits a standardized uniform dispersion of the inorganic nanofillers (Shetty et al. 2019).

EDS analysis gives the basic structure and uniform distribution of nanofillers TiO_2 and ZnO in host polymer PMMA. Initially, the PMMA nanocomposite films were sputtered primarily by using gold ions to resist the artifacts created above the film surface. Figure 10 identifies the proportion of nano-sized TiO_2 and ZnO nanofillers distributed in the PMMA nanocomposites.

SEM performed elemental mapping of nanofillers to confirm the dispersion of Ti, Zn, S, and O in the surface of the PMMA nanocomposites. Figure 11 shows the elemental mapping in various colors such as O (green), Zn

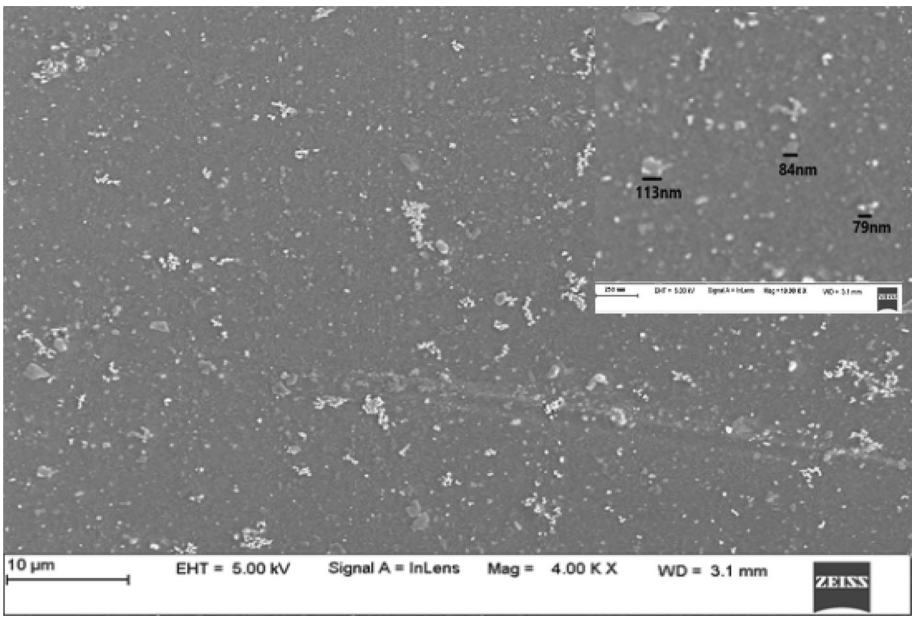

Fig. 9 SEM image of PMMA filled with x = 10wt% of $(15 - x)$ ZnO and (x) TiO_2 nanofillers

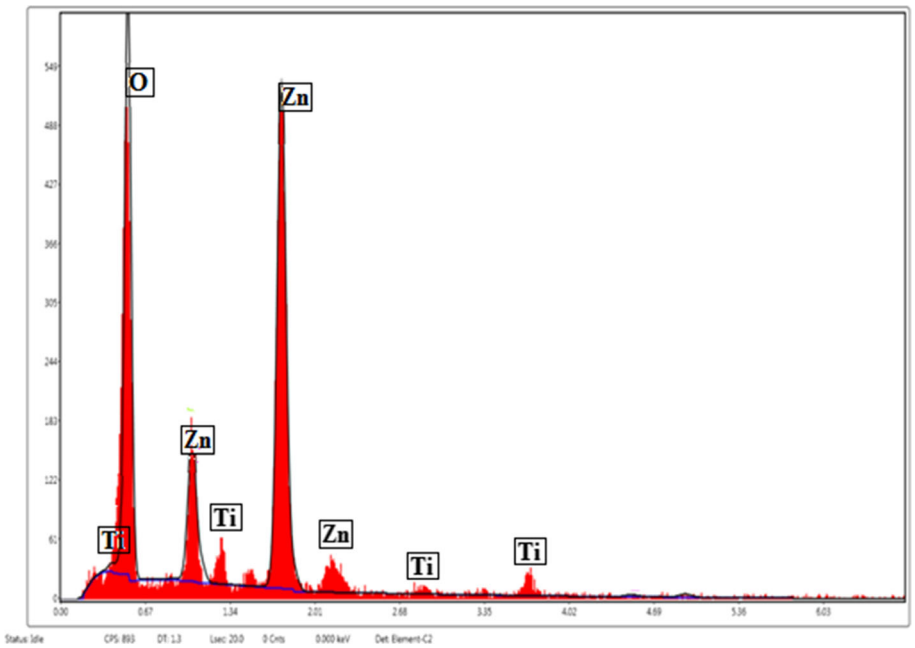

Fig. 10 EDS graph indicating the distribution of nanofillers in the PMMA matrix for x = 10wt%

(blue), Ti (brown), and S(red), respectively. The elemental mapping also signifies the homogenous distribution of nanofillers in the PMMA nanocomposites.

4 Conclusion

A simple spin coating method is successfully employed to obtain PMMA: $(15 - x)$ ZnO (x) TiO_2 hybrid nanocomposites. The transformation of thin layer nano-hybrid film on a glass substrate was analyzed for morphological, functional, and chemical effects. XRD studies indicate that nanoparticles' addition into the PMMA matrix shifts the PMMA peaks toward the lower angle. An increase in the crystalline peak for x = 10 wt% indicates the enhancement in crystalline properties. The FESEM shows the compatibility and homogenous distribution of added nanofillers ZnO and TiO_2 with the host PMMA matrix. The Raman spectroscopy identifies the shifts in the peaks heading toward the lower wavelength indicate the complex formation of nanofillers on PMMA's C–O and C=O bond, making it out of plane bending with PED of every normal mode $55\eta_{C-O} + 11\eta_{C=O}$. The prominent transition peak witnessed at 840 cm^{-1} for optimized filler concentration

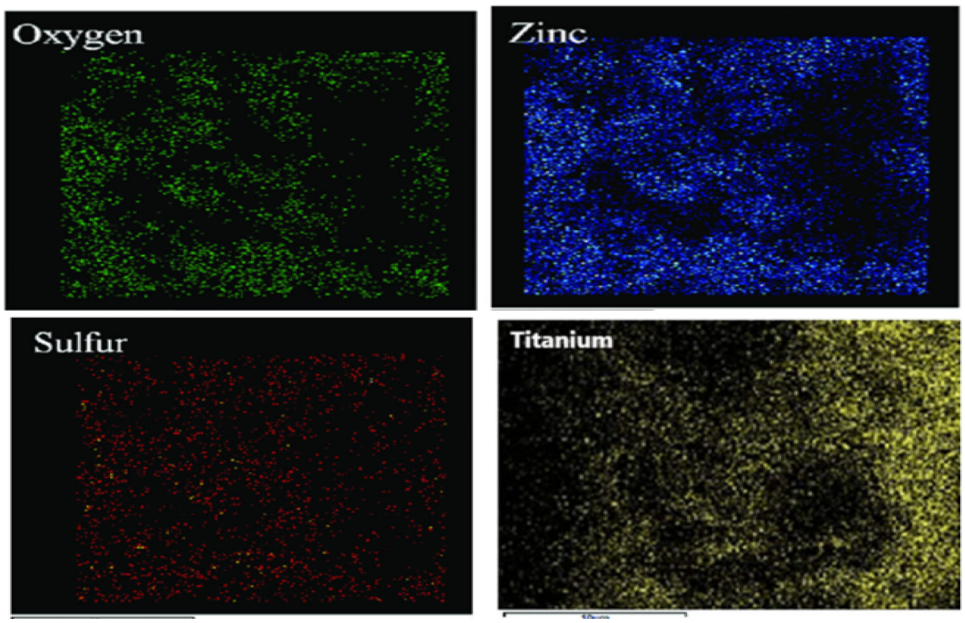

Fig. 11 The elemental mapping of nanofillers in the PMMA matrix for x = 10wt% filler concentration

x = 10 wt% refers to C=O and C–O out of plane bending with an estimated PED of $64\eta_{C=O} + 16\eta_{C-O}$. The transmittance spectra of UV–visible spectroscopy of filled PMMA/$(15 - x)$ ZnO (x) TiO_2 compared with unfilled PMMA shows an enhancement in transmittance in filler concentration up to 10 wt% offering a maximum value of nearly 85% and decreased energy gap of 1.91 eV. The optical conductivity found maximum in UV and the visible region for optimum filler concentration of x = 10 wt% makes the material PMMA/$(15 - x)$ZnO(x) TiO_2 for applications in optical devices.

Acknowledgements The authors are grateful to the Visvesvaraya Technological University, Belgavi, Karnataka [Project Sanction No. Ref. VTU/TEQIP-3/2020/422 date 18/01/ 2020], providing financial support under the VTU-TEQIP Competitive Research Funding scheme. The authors also like to thank the Ministry of education in Saudi Arabia and Taif University Researchers Supporting Project Number (TURSP- 2020/47), Taif University, Taif, Saudi Arabia.

Declarations

Conflict of interest There are no conflicts of interest to declare.

References

Abdul-Gader JM (2013) Temperature dependence of DC conductivity of as-deposited and annealed selenium films Europ Int J. Sci Technol 2:214–274. https://doi.org/10.1080/002072198134328

Aboulouard A, Gultekin B, Can M, Erol M, Jouaiti A, Elhadadi B, Zafer C, Demic S (2020) Dye-sensitized solar cells based on titanium dioxide nanoparticles synthesized by flame spray pyrolysis and hydrothermal sol-gel methods: a comparative study on photovoltaic performances. J Mater Res Technol 9:1569–1577. https://doi.org/10.1016/j.jmrt.2019.11.083

Agarwal S, Kulshrestha V, Saraswat VK (2014) Thermal optical and mechanical characterization of ZnO embedded PC/PMMA blend nanocomposites. Int J Sci Amp Technol 2:140–144

Al-Ammar K, Hashim A, Husaien M (2013) Synthesis and study of optical properties of (PMMA-$CrCl_2$). Compos Chem Mater Eng 1:85–87. https://doi.org/10.13189/cme.2013.010304

Alsaad AM, Al-Bataineh QM, Ahmad AA, Jumh I, Alaqtash N, Bani-Salameh AA (2019) Optical properties of transparent PMMA-PS/ZnO NPs polymeric nanocomposite films: UV-Shielding applications. Mater Res Express 6:126446

Bai Y, Sero IM, de Angelis F, Bisquert J, Wang P (2014) Titanium dioxide nanomaterials for photovoltaic applications. Chem Rev 114:10095–10130. https://doi.org/10.1021/cr400606n

Basahel SN, Ali TT, Narasimha Rao K, Bagabas AA, Mokhtar M (2012) Effect of iron oxide loading on the phase transformation and physicochemical properties of nano-sized mesoporous ZrO2. Mater Res Bull 47(11):3463–3472

Bhajantri RF, Ravindrachary V, Harisha A, Crasta V, Suresh Nayak P, Poojary B (2006) Microstructural studies on BaCl2 doped Poly (vinyl alcohol). Polymer 47:3591–3598. https://doi.org/10.1016/j.polymer.2006.03.054

Chang T, Kim C, Hwang C (eds) (2011) INTER-NOISE and NOISE-CON congress and conference proceedings institute of noise control engineering

Choudhary RB, Nayak D (2019) Tailoring the properties of 2-D rGO-PPy-ZnS nanocomposite as an emissive layer for OLEDs. Opt Mater 91:470–481. https://doi.org/10.1016/j.ijleo.2021.166336

de Vos A, van Dhelsen D (1979) The temperature dependence of the electrical properties of thin tellurium films. Rev Phys Appl 14:815–820. https://doi.org/10.1051/rphysap:01979001409081500

Dette C, Pérez-Osorio MA, Kley CS, Punke P, Patrick CE, Jacobson P, Giustino F, Jung SJ, Kern K (2014) TiO_2 anatase with a bandgap in the visible region. Nano Lett 14:6533–6538. https://doi.org/10.1021/nl503131s

Di Mauro A, Cantarella M, Nicotra G, Privitera V, Impellizzeri G (2016) Low temperature atomic layer deposition of ZnO: applications in photo catalysis. Appl Catal B Environ 196:68–76. https://doi.org/10.1016/j.apcatb.2016.05.015

Di Mauro A, Cantarella M, Nicotra G, Pellegrino G, Gulino A, Brundo MV, Privitera V, Impellizzeri G (2017) Novel synthesis

of ZnO/PMMA nanocomposites for photocatalytic applications. Sci Rep 7:40895. https://doi.org/10.1038/srep40895

Giri PK, Bhattacharyya S, Singh DK, Kesavamoorthy R, Panigrahi BK et al (2007) Correlation between microstructure and optical properties of ZnO nanoparticles synthesized by ball milling. J Appl Phy 102:093515. https://doi.org/10.1063/1.2804012

Hong W, Woo H-J, Choi H-W, Kim Y-S, Kim G-D (2009) Optical property modification of PMMA by ion-beam implantation. Appl Surf Sci 169:428–432. https://doi.org/10.1016/S0169-4332(00)00698-X

Huda B, Khaleel A, Mohammed H, Hashem A (2019) Cooling Solar Cells Using ZnO Nanoparticles as a down-Shifter. Therm Sci 24:809–814. https://doi.org/10.2298/TSCI180324004B

Khan SS (2015) Enhancement of visible light photocatalytic activity of CdO modified ZnO nanohybrid particles. Photochem Photobiol B 142:1–7. https://doi.org/10.1016/j.jphotobiol.2014.11.001

Khanna PK, Singh N, Charan S (2007) Synthesis of nanoparticles of anatase-TiO2 and preparation of its optically transparent film in PVA. Mater Lett 61:4725–4730. https://doi.org/10.1016/j.matlet.2007.03.064

Kobayashi Y, Kurosawa A, Nagao D, Konno M (2009) Fabrication of barium titanate nanoparticles-PMMA composite films and their dielectric properties. Polym Eng Sci 49(6):1069–1075

Kumar S, Rath T, Khatua BB, Dhibar AK, Das CK (2009) Preparation and characterization of poly(methyl methacrylate)/multi-walled carbon nanotube composites. J Nanosci Nanotechnol 9(8):4644–4655

Lim ES, Lee JC, Kim JJ, Park ET, Chung YK, Lee HY (2005) Dielectric characteristics of polymer ceramic-metal composites to apply embedded passive devices. Integr Ferroelectr 74(1):53–60

Mardare D, Rusu GI (2004) Comparison of the dielectric properties for doped and undoped tio$_2$ thin films. J Optoelectron Adv Mater 6:333–336

Mott NF (1993) Conduction in non-crystalline materials, 2nd edn. Clarendon Press, Oxford

Mott NF, Devis EA (1979) Electronic process in non-crystalline materials, 2nd edn. Oxford University Press, Oxford

Patil AV, Dighavkar CG, Sonawane SK (2009) Effect of firing temperature on electrical and structural characteristics of screen printed ZnO thick films Optoelectron. Adv Mater Rapid Commun 3:879–883

Purova R, Narasimharao K, Ahmed NSI, Al-Thabaiti S, Al-Shehri A, Mokhtar M, Schwieger W (2015) Pillared HMCM-36 zeolite catalyst for biodiesel production esterification of palmitic acid. J Mol Catal A Chem 406:159–167

Rosemal HM, Harisa SM, Kathiresanb S (2010) FT-IR and FT-raman spectra and normal coordinate analysis of polymethyl methacrylate. Der Pharma Chem 2:316–323

Rouaramadan E, Hasan AA (2013) Int J Appl Innovat Eng Manage 2: 240–245

Selim MS, Seoudi R, Shabaka AA (2005) Polymer-based films embedded with high content of ZnSe nanoparticles. Mater Lett 59:2650–2654. https://doi.org/10.1016/j.matlet.2005.04.012

Shetty BG, Vincent C, Kumar NBR, Rajesh K, Bairy R, Shankaragouda PP (2019) Cobalt doping in tuning the bandgap, surface morphology and third-order optical nonlinearities of ZnO nanostructures for NLO device applications. Opt Mater 95:109218. https://doi.org/10.1039/C9RA03006A

Stefanescu EA, Tan X, Lin Z, Bowler N, Kessler MR (2010) Multifunctional PMMA-Ceramic composites as structural dielectrics. Polymer 51:5823–5832

Su K, Jiang F, Qian J, Gai Y, Wu M, Bawaked SM, Mokhtar M, AL-Thabaiti SA, Hong M (2014) Generalized Synthesis of Calixarene-Based High-Nuclearity M_{4n} Nanocages (M = Ni or Co; n = 2–6). Cryst Growth Des 14(6):3116–3123

Tauc J (1972) Optical properties of solids. In: Abeles F (ed) Optical Properties of Solid. vol 277. North-Holland, Amsterdam, The Netherlands

Williamson GB, Smallman RC (1956) III dislocation densities in some annealed and cold-worked metals from measurements on the X-ray Debye-Scherrer spectrum. Phil Mag 1:34–46. https://doi.org/10.1080/14786435608238074

Zidan HM (2003) Structural properties of CrF3- and MnCl2-filled Poly (vinyl alcohol) films. J Appl Polym Sci 88:1115–1120. https://doi.org/10.1002/app.12123